nature communications

Article

https://doi.org/10.1038/s41467-025-65949-9

Identification of overoxidizing and non-overoxidizing NAD-dependent methanol dehydrogenases and implications for synthetic methylotrophy

Received: 24 January 2025

Accepted: 28 October 2025

Published online: 09 December 2025

Check for updates

Philipp Keller[1,4] ✉, Emese Hegedis[1,4], Benedikt Jäger[1], Simon H. Rüdisser[2], Hedwig Schultz[1], Lars A. Büchel[1], Andrea M. Ochsner[1], Timothy Bradley[1], Michael A. Reiter[1], Donald Hilvert[3] & Julia A. Vorholt[1] ✉

Synthetic methylotrophy offers opportunities for sustainable chemical and biofuel production. While recently established methylotrophic *E. coli* can grow on methanol, undesirable formate accumulation occurs during growth and bioproduction. Here, we show that NAD-dependent methanol dehydrogenase Mdh2 from *Cupriavidus necator* inherently overoxidizes methanol to formate, a trait we find to be widespread among NAD-dependent Mdh enzymes. In contrast, Mdh/Mdh1 enzymes from *Bacillus methanolicus* exclusively oxidize methanol to formaldehyde without overoxidation, as we validate in vitro for Mdh Bm MGA3 with and without activator protein Act. Since only formaldehyde is assimilated via the ribulose monophosphate pathway, this explains the physiological role of Mdh/Mdh1 paralogs in natural methylotrophs and highlights the importance of selecting appropriate Mdh variants for synthetic methylotrophy. We demonstrate methanol-dependent growth using non-overoxidizing Mdh Bm MGA3, strongly reducing formate accumulation and carbon loss. Our findings reveal a characteristic of NAD-dependent Mdh enzymes and provide insights for engineering synthetic methylotrophs.

The release of greenhouse gases (GHG) from anthropogenic sources over the last two centuries has caused a global climate crisis, driving the need for sustainable approaches to mitigate GHG emissions[1–3]. The chemical industry is a major contributor, accounting for approximately 5% of global GHG emissions[4]. Achieving a zero-emission chemical industry requires the replacement of fossil feedstocks with CO_2-based alternatives. Among these, the one-carbon compound methanol is an attractive sustainable feedstock because it can be produced renewably from GHG (e-methanol) or biomass (bio-methanol) at scale and at competitive costs[5].

Biological cell factories have attracted increasing interest for converting methanol into a wide range of value-added products. Natural methylotrophs, which have been studied intensively over many decades[6], have been used and engineered for methanol-based production[7–18]. Substantial progress has been made; however, they have not yet been adopted in large-scale industrial processes[19,20]. As an alternative approach to establishing a versatile platform for the biosynthesis of products from methanol, great advances have been achieved in converting the well-established industrial workhorse *Escherichia coli* into a synthetic methylotroph[21–27]. To date, four

[1]Institute of Microbiology, Department of Biology, ETH Zurich, Zurich, Switzerland. [2]Biomolecular NMR Spectroscopy Platform, Department of Biology, ETH Zurich, Zurich, Switzerland. [3]Laboratory of Organic Chemistry, ETH Zurich, Zurich, Switzerland. [4]These authors contributed equally: Philipp Keller, Emese Hegedis. ✉e-mail: kellerp@ethz.ch; jvorholt@ethz.ch

independently engineered and evolved *E. coli* strains have been reported that are capable of growing on methanol as sole carbon source[28–31].

The first metabolic step shared by all methylotrophic bacteria for growth on methanol is its oxidation to formaldehyde. This reaction is commonly carried out by either an NAD-dependent methanol dehydrogenase (Mdh) in Gram-positive bacteria[32] or pyrroloquinoline quinone (PQQ)-dependent Mdh in Gram-negative bacteria[6]. All synthetically engineered methylotrophic *E. coli* strains described to date employ NAD-dependent Mdh as the methanol-oxidizing enzyme[28–31]. The choice of an NAD-dependent enzyme is justified by its ease of expression in *E. coli* and by the cell's ability to utilize NADH in its electron transport chain. Because this enzyme has a relatively low turnover and affinity for methanol, various NAD-dependent Mdh enzymes have been explored in the context of synthetic methylotrophy in *E. coli*, including *Cupriavidus necator* Mdh2[24,26,28,29,31,33,34], *Geobacillus stearothermophilus* Mdh[28,35–38], *Lysinibacillus xylanilyticus* Mdh[39,40] and methanol dehydrogenases from *Bacillus methanolicus* sp[21–23,28,41].

To channel formaldehyde generated from methanol oxidation into central carbon metabolism, the ribulose monophosphate (RuMP) cycle has been introduced into *E. coli*[29,30]. This highly efficient pathway requires the heterologous expression of only two additional genes, 3-hexulose 6-phosphate synthase (*hps*) and 6-phospho 3-hexuloisomerase (*phi*). In this pathway, formaldehyde condenses with ribulose 5-phosphate to form hexulose 6-phosphate, thereby directly integrating the toxic intermediate into biomass and potential products.

As a proof-of-principle for methanol-based bioproduction, we recently showed the production of four industry-relevant compounds using a synthetic methylotrophic *E. coli* strain[42]. For a bioprocess to be both economic and efficient, methanol must be channeled into the product with minimal generation of unwanted by-products. However, synthetic methylotrophic *E. coli* strains were found to accumulate significant amounts of formate (up to more than 10 mM) during aerobic growth in the absence of *E. coli*'s native glutathione-dependent formaldehyde detoxification pathway that natively oxidizes formaldehyde to formate[27,29,43]. In synthetic methylotrophy, this detoxification pathway is commonly inactivated to direct carbon flux towards biomass[21,22,25,27,34,36,37,43]. Even if not deliberately turned off, this pathway is (often) spontaneously inactivated when the strain is evolved for methanol-dependent growth[23,24,29], underlining the need to conserve formaldehyde for assimilation.

In this study, by initially investigating the origin of formate accumulation in a synthetic methylotrophic *E. coli* strain grown on methanol, we discover that NAD-dependent Mdh enzymes not only generate formaldehyde but also overoxidize methanol to formate. By screening a variety of NAD-dependent Mdh enzymes, we find that overoxidation is widespread but not universal among these enzymes. *B. methanolicus* MGA3 Mdh (Mdh Bm MGA3) as well as *B. methanolicus* PB1 Mdh and Mdh1 (Mdh/Mdh1 Bm PB1) do not convert methanol to formate. These enzymes have been previously classified as "Mdh/Mdh1" based on their sequence identity, in contrast to "Mdh2/Mdh3" enzymes (Mdh2 and Mdh3 Bm MGA3 and Mdh2 Bm PB1)[44]. Our findings offer a plausible explanation for the presence of multiple *mdh* genes in *B. methanolicus*. Additionally, we demonstrate that introducing a non-overoxidizing Mdh reduces formate accumulation in *E. coli* during methanol-dependent growth, offering a starting point for improving bioproduction from methanol.

Results

Synthetic methylotrophic *E. coli* accumulates formate as a side-product during growth

First, we confirmed that formate is produced by the synthetic methylotrophic *E. coli* strain MEcoli_ref_2 previously described[42]. When grown in a bioreactor on methanol, we observed formate in the mM range (~3 mM, 138 mg L^{-1}) (Supplementary Fig. 1a, Supplementary Data 1). Even higher concentrations of formate, up to 38 mM, accumulated during the production of itaconic acid or lactic acid from methanol (Supplementary Fig. 1b, c, Supplementary Data 2). Because the synthetic methylotrophic *E. coli* strain underwent adaptive laboratory evolution (ALE) over approximately 1200 generations, we tested whether formate production also occurs in its ancestral methanol-dependent strain (Δ*frmA*Δ*tpiA*) which heterologously expresses *mdh*, *hps*, and *phi*[26,30]. This ancestral strain likewise produced formate (~8 mM) (Fig. 1a, Supplementary Data 3), indicating that formate generation is intrinsic to the strain rather than the result of ALE toward methylotrophic growth.

The metabolic origin of formate in the absence of *frmA*, which encodes *S*-(hydroxymethyl)glutathione dehydrogenase in the formaldehyde detoxification pathway, remained unclear. To determine whether formate originates from a metabolite close to the one-carbon entry point into the RuMP cycle, we investigated the methanol-dependent strain under defined conditions in which overall carbon flux from methanol and pyruvate is well characterized and consistent with flux balance analysis[26]. By feeding ^{13}C-labeled methanol and unlabeled pyruvate, we could trace the origin of formate through its labeling pattern (Fig. 1b). More than 95% of the formate originated from methanol (Fig. 1c, Supplementary Data 4), indicating that it derives from either formaldehyde or a RuMP cycle intermediate close to the one-carbon entry point.

One potential mechanism for formate generation would be the activity of an alternative dehydrogenase that compensates for the lack of *frmA* in the strain. To investigate this possibility, we deleted the entire formaldehyde detoxification pathway operon (Δ*frmRAB*). However, these deletions did not abolish formate production (Supplementary Fig. 2, Supplementary Data 5–10), indicating another route for formate production by the synthetic methylotrophic *E. coli*.

NAD-dependent methanol dehydrogenase Mdh2 CT4-1 Cn oxidizes formaldehyde to formate in vitro

Another potential route for the direct oxidation of formaldehyde to formate involves the heterologously introduced methanol dehydrogenase itself, here Mdh2 CT4-1 Cn[45]. In aqueous solution, formaldehyde exists predominantly as methylene glycol[46–49] (Supplementary Fig. 3), a form that could be recognized as a substrate by methanol dehydrogenase, which has a broad substrate specificity[45].

To investigate whether Mdh2 CT4-1 Cn oxidizes formaldehyde to formate, we purified the enzyme from an *E. coli* BL21 overexpression culture and characterized it in vitro. We monitored the initial rate of NADH formation upon addition of formaldehyde to a reaction mixture containing Mdh and NAD^+ at 37 °C. Indeed, a sharp increase in NADH was observed immediately after the addition of formaldehyde (Fig. 2a), confirming that the enzyme catalyzes the oxidation of formaldehyde to formate, while reducing NAD^+ to NADH. As expected, NADH formation was also observed when the reaction was started from methanol (Fig. 2b). Further experiments at varying substrate concentrations revealed that formaldehyde oxidation proceeds with substantially higher turnover rates than methanol oxidation (Fig. 2c, single traces in Supplementary Fig. 4). For the reverse reactions, only activity from formaldehyde to methanol but not from formate to formaldehyde was observed (Supplementary Fig. 5). These findings demonstrate that Mdh2 CT4-1 Cn overoxidizes methanol to formate and suggest that Mdh is responsible for formate production by methanol-dependent and synthetic methylotrophic *E. coli* strains.

Overoxidation of methanol by NAD-dependent methanol dehydrogenases is common

To examine whether overoxidation is a general feature of NAD-dependent Mdh, we overexpressed nine different NAD-dependent

https://doi.org/10.1038/s41467-025-65949-9

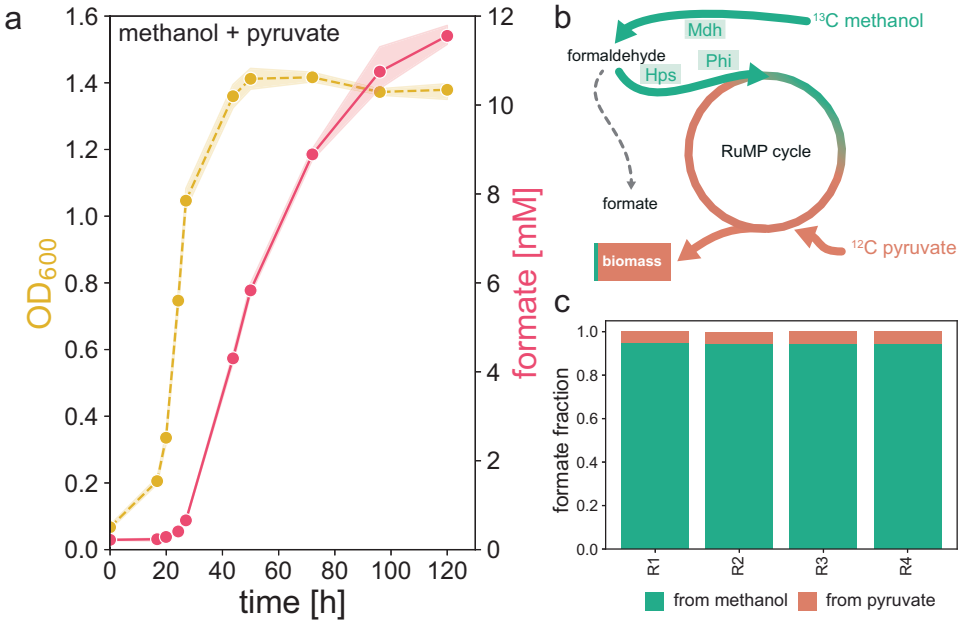

Fig. 1 | Formate production and isotopic tracer analysis of methanol-dependent strain Δ*frmA*Δ*tpiA*. **a** Optical density (OD) and formate production of the methanol-dependent strain Δ*frmA*Δ*tpiA* expressing *mdh*, *hps*, and *phi* during growth on methanol (500 mM) and pyruvate (20 mM) in shake flasks ($n = 3$). The mean of the data is shown as solid line and the shaded regions represent the range of the 95% confidence intervals. **b** Simplified metabolic scheme illustrating methanol-dependent growth of *E. coli* Δ*frmA*Δ*tpiA* expressing *mdh*, *hps*, and *phi* when cultivated on methanol and pyruvate. Molecules originating from formaldehyde or close to the one-carbon entry point are expected to be formed from methanol (green) while others are formed from pyruvate (orange). The canonical formaldehyde detoxification pathway of *E. coli*, which should not be active in the methanol-dependent strain due to its *frmA* deletion, is indicated in gray. **c** Fraction of formate molecules determined in the supernatant of the methanol-dependent strain originating from ^{13}C methanol (green) and ^{12}C pyruvate (orange) when sampled at stationary phase. R1-R4 indicate replicate experiments. Source data are provided as a Source Data file.

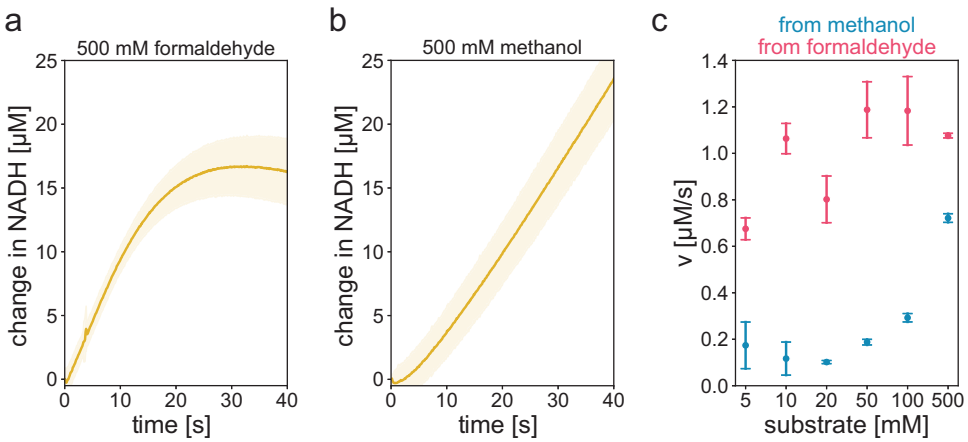

Fig. 2 | Overoxidation of methanol to formate is catalyzed by Mdh2 CT4-1 Cn. In vitro assays of Mdh2 CT4-1 Cn showing the initial change in NADH concentration by monitoring the absorption at 340 nm. Reactions contained 12.3 µM enzyme, 5 mM NAD^+ and were started by the addition of 500 mM formaldehyde (**a**) or methanol (**b**), respectively. The mean of the data is shown as solid line and the shaded region represents the range of the 90% confidence interval. **c** Rate of NADH formation in the presence of 10, 20, 50, 100 and 500 mM methanol or formaldehyde. Methanol to formaldehyde reactions are indicated in blue, formaldehyde to formate in red. Experiments were performed in triplicates and data are represented as mean ± the standard deviation. Source data are provided as a Source Data file.

Mdh enzymes in an *E. coli* strain lacking its canonical formaldehyde detoxification pathway (Δ*frmRAB*). When grown on pyruvate supplemented with methanol as substrate for Mdh, six of these enzymes produced more than 4 mM formate, whereas in the other three strains formate accumulation was below 600 µM (Fig. 3a, Supplementary Fig. 6 and Supplementary Data 11 for time course data).

Multiple sequence alignment and phylogenetic analysis revealed that the non-overoxidizing enzymes form a separate cluster, sharing less than ~70% sequence identity with the remaining enzymes (Fig. 3b). This cluster has previously been described as Mdh/Mdh1 in *B. methanolicus* strains[44], where these enzymes represent the predominant methanol dehydrogenase[32,44]. The physiological relevance of this enzyme cluster was not previously elucidated[44,50], but the observed non-overoxidation of methanol, in contrast to other Mdh enzymes, may be a hallmark of this class of Mdh enzymes.

To further expand the range of Mdh enzymes investigated, we generated a phylogenetic tree based on the top 1000 hits from a BLAST search using Mdh Bm MGA3 against the NCBI database (Supplementary Fig. 7). Eight additional Mdh enzymes, representing different phylogenetic branches, were selected for testing based on their

https://doi.org/10.1038/s41467-025-65949-9

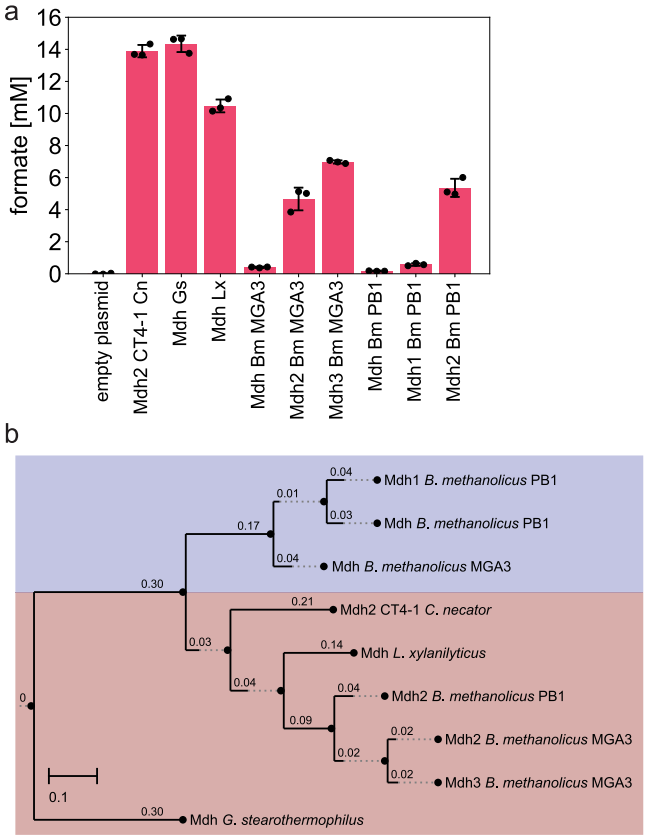

Fig. 3 | NAD-dependent methanol dehydrogenases fall in two groups/clades, overoxidizing and non-overoxidizing enzymes, based on in vivo screening. **a** Formate production by different NAD-dependent methanol dehydrogenases. Strains overproducing Mdh in *E. coli* (Δ*frmRAB*) were grown on methanol (500 mM) and pyruvate (20 mM) and formate was quantified in the supernatant of the cultures after 69 h. The formate levels of a strain harboring an empty plasmid were used as background control and subtracted from each measured value. Experiments were performed in triplicates and data are represented as mean ± the standard deviation. **b** Mdh enzymes that do (>4 mM, red) and do not (Mdh/Mdh1, blue) overoxidize methanol form separate phylogenetic clusters. Source data are provided as a Source Data file.

confirmed methanol dehydrogenase activity[27]. All of these showed significant formate production, confirming that overoxidation is widespread among Mdh enzymes (Supplementary Fig. 8, Supplementary Data 12). We also included Mdh from *B. methanolicus* strain C1 in this experiment, which has been characterized biochemically in previous studies[51–53]. Consistent with other enzymes in the Mdh/Mdh1 cluster, no formate production was detected for Mdh Bm C1.

Mdh Bm MGA3 does not oxidize formaldehyde in vitro

The in vivo Mdh screen identified three candidate methanol dehydrogenases that reduce formate accumulation in vivo. To further validate that these Mdh enzymes do not overoxidize methanol to formate, we purified one of these enzymes, Mdh Bm MGA3, from an *E. coli* BL21 overexpression culture for in vitro assays. Strikingly and in contrast to Mdh2 CT4-1 Cn (Fig. 2a), when formaldehyde (500 mM) was used as a substrate to start the reaction, no NADH formation was detected, confirming that this Mdh does not oxidize formaldehyde (Fig. 4a). When starting the reaction with the same concentration of methanol, NADH formation was observed as expected (Fig. 4b)[44]. In comparison to Mdh2 CT4-1 Cn, the turnover rate for the oxidation of methanol by Mdh Bm MGA3 was about seven times slower, which is in line with previous reports due to the inferior catalytic efficiency and difference in temperature optimum of Mdh Bm MGA3[44,45]. Because 500 mM formaldehyde might inactivate the enzyme, we also tested lower initial formaldehyde concentrations (5–500 mM) and confirmed that the enzyme was not inactivated by the formaldehyde by subsequently adding methanol and monitoring its oxidation (Supplementary Fig. 9). In all cases, Mdh MGA3 showed no detectable activity (Fig. 4c, for single traces see Supplementary Fig. 10). Furthermore, as observed for Mdh2 CT4-1 Cn, Mdh Bm MGA3 catalyzed the reverse reaction from formaldehyde to methanol but not the reduction of formate to formaldehyde (Supplementary Fig. 11).

NAD-dependent methanol dehydrogenases are known to show apparent activation by Nudix hydrolases in vitro[21,44,51,52,54], a phenomenon recently attributed to the removal of ADP-ribose, an inhibitor formed during NAD^+ hydrolysis[55]. We wondered whether the addition of the Nudix hydrolase Act from *B. methanolicus* would enable formaldehyde oxidation by Mdh Bm MGA3. To investigate this, we purified Act from a BL21 *E. coli* overexpression culture and repeated the in vitro assay in its presence. However, no NADH was generated when the reaction was started with formaldehyde in the presence of Act, regardless of whether the assay was performed both at the optimal

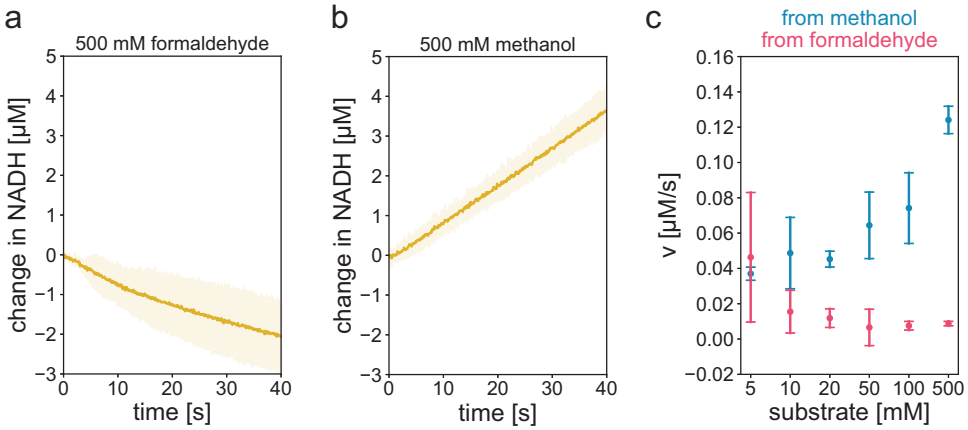

Fig. 4 | Mdh Bm MGA3 does not catalyze the overoxidation of methanol to formate. In vitro assays of Mdh Bm MGA3 showing the initial change in NADH concentration by monitoring the absorption at 340 nm. Reactions contained 12.5 µM enzyme, 5 mM NAD^+ and were started by the addition of 500 mM formaldehyde (**a**) or methanol (**b**), respectively. The mean of the data is shown as solid line and the shaded regions represent the range of the 90% confidence intervals. **c** Rate of NADH formation in the presence of 10, 20, 50, 100, and 500 mM methanol or formaldehyde. Methanol to formaldehyde reactions are indicated in blue, formaldehyde to formate in red. Experiments were performed in triplicates and data are represented as mean ± the standard deviation. Source data are provided as a Source Data file.

https://doi.org/10.1038/s41467-025-65949-9

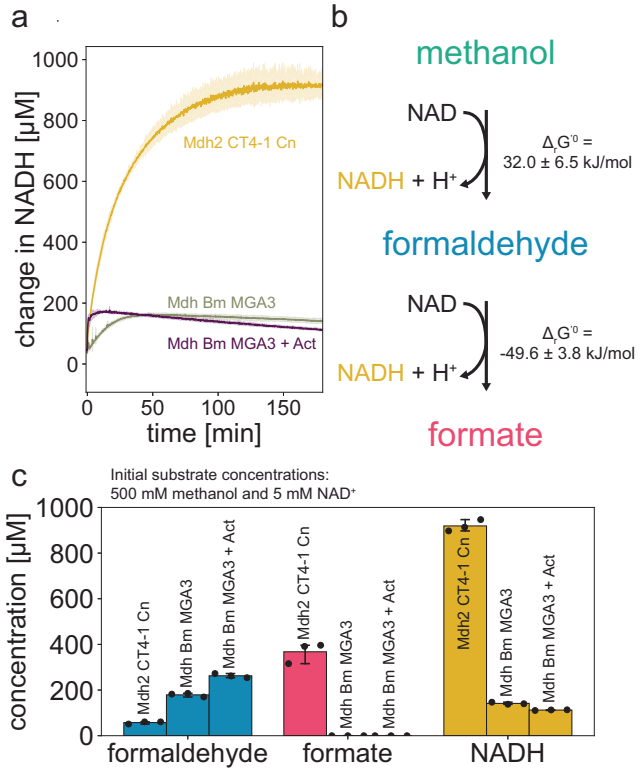

Fig. 5 | Metabolite concentrations at equilibrium differ between overoxidizing Mdh2 CT4-1 Cn and non-overoxidizing Mdh Bm MGA3. a In vitro assays of Mdh2 CT4-1 Cn (yellow), Mdh Bm MGA3 (olive green), and Mdh Bm MGA3 + Act (purple) monitored until equilibrium was reached. Reactions contained 25 µM Mdh2 CT4-1 Cn or 25 µM Mdh Bm MGA3, 2.3 µM Act if indicated, 5 mM NAD^+ and were started by the addition of 500 mM methanol. The mean of the data is shown as solid line and the shaded regions represent the range of the 90% confidence intervals. **b** Methanol oxidation to formaldehyde and its subsequent oxidation to formate. $\Delta_rG'^0$ values were calculated by Equilibrator (pH = 7.4, pMg = 2.3, ionic strength = 0.15 M)[96,101]. **c** Equilibrium concentrations of formaldehyde (blue), formate (red), and NADH (yellow). Reactions contained 25 µM Mdh2 CT4-1 Cn or 25 µM Mdh Bm MGA3, 2.3 µM Act if indicated, 5 mM NAD^+ and were started by the addition of 500 mM methanol. Experiments were performed in triplicates and data are represented as mean ± the standard deviation. Source data are provided as a Source Data file.

growth temperature of *E. coli* (37 °C) or that of *B. methanolicus* (50 °C) (Supplementary Fig. 12).

Thermodynamic equilibrium analyses validate the ability of Mdh Bm MGA3 to exclusively oxidize methanol to formaldehyde

We further validated the equilibrium states of the in vitro reactions for both an overoxidizing (Mdh2 CT4-1 Cn) and non-overoxidizing Mdh (Mdh Bm MGA3). In these experiments, 500 mM methanol, 5 mM NAD^+, and 25 µM Mdh2 CT4-1 Cn or 25 µM Mdh Bm MGA3 were incubated beyond the initial reaction phase until equilibrium was reached. We also tested Mdh Bm MGA3 in the presence of Act. As expected, the time to reach equilibrium varied substantially for the different conditions, with Mdh Bm MGA3 in the presence of Act requiring the shortest time due to its higher catalytic activity[21,44,51,52,54].

Consistent with the one versus two-step oxidation process (methanol → formaldehyde → formate), the final NADH levels differed markedly between the overoxidizing and non-overoxidizing Mdh enzymes (900 vs 140 µM formed NADH), irrespective of Act addition (Fig. 5a). Thermodynamic calculations based on the Gibbs free energy under standard conditions for methanol oxidation to formaldehyde ($\Delta G_r'^0 = 32.0 \pm 6.5$ kJ/mol) and formaldehyde oxidation to formate ($\Delta G_r'^0$ of -49.6 ± 3.8 kJ/mol) (Fig. 5b) predicted roughly 100 µM for the non-overoxidizing reaction under the experimental conditions, closely matching the observed value (Fig. 5c). For an overoxidizing Mdh, the calculated NADH concentration was close to 5 mM which is higher than what was measured (920 µM). Similarly, measured formaldehyde and formate concentrations at equilibrium deviated from theoretical values in the overoxidizing reaction (57 µM vs 0.01 µM formaldehyde and 368 µM vs 2.5 mM formate), suggesting constraints such as limited affinity for formaldehyde or incomplete equilibration in the experimental timeframe, potentially due to inactivation of the enzyme by formaldehyde. Nevertheless, these findings further support the inability of Mdh Bm MGA3 to oxidize formaldehyde.

Sequence alignment reveals conserved residues in overoxidizing and non-overoxidizing Mdh enzymes

We were further wondering whether specific regions of the Mdh enzymes could be attributed to the ability or inability of methanol overoxidation. To compare the overoxidizing to the non-overoxidizing Mdh class, we performed a multiple sequence alignment (MSA) with the sequences of the enzymes tested in the Mdh screen (Fig. 6, Supplementary Fig. 13). The sequences showed sufficient similarity to produce a gapless alignment. The presumed residues interacting with the cofactor NAD(P)(H) and metal ion coordinating residues, based on structurally characterized type III alcohol dehydrogenases (Adhs)[56–60], are mostly conserved among all sequences.

When comparing the overoxidizing and non-overoxidizing Mdh group sequences, 24 residues were found to be conserved within the respective groups. These residues are distributed across the alignment and do not form any obvious clusters in the sequence. To gain insight into the relevance of these possibly characteristic residues, we predicted the structures of Mdh2 CT4-1 Cn and Mdh Bm MGA3 as representative examples for the two groups (Supplementary Fig. 14). In accordance with the solved structures of other group III Adhs[56–60], the predictions indicate the formation of two domains with a deep cleft in between, containing the cofactor binding sites. Similar to the sequence alignment, the residues of interest are dispersed across the two domains, however showing some aggregation around the active site cleft. This supports the hypothesis that the identified 24 residues might be relevant for the distinction between methanol and formaldehyde as substrates for oxidation. The specific role of each of these residues, however, is yet to be determined and will require more in-depth knowledge about the catalytic mechanism of the enzymes.

Replacement of overoxidizing with non-overoxidizing methanol dehydrogenase reduces the accumulation of formate during methanol-dependent growth

The in vivo and in vitro experiments described above showed that Mdh Bm MGA3, unlike other Mdh enzymes, does not oxidize formaldehyde. This finding identifies Mdh/Mdh1-type enzymes as promising candidates for synthetic methylotrophic *E. coli* strains, in which only overoxidizing Mdh enzymes have been used to date[28–31,42]. Since it is crucial to minimize the unwanted production of formate and to maintain a pool of formaldehyde for assimilation purposes, we tested whether a non-overoxidizing Mdh sustains growth of *E. coli* in the presence of methanol without causing the accumulation of formate. We exchanged the overoxidizing Mdh2 CT4-1 Cn in the synthetic methylotrophic *E. coli* strain MEcoli_ref_2 with Mdh Bm MGA3. We cured the strain from its plasmid containing *mdh2* CT4-1 Cn and reintroduced a new plasmid containing *mdh* Bm MGA3. However, no growth on methanol was observed under our experimental conditions. As a control, retransformation of the cured strain with the original plasmid containing *mdh2* CT4-1 Cn restored growth on methanol, suggesting that MEcoli_ref_2's metabolism had adapted to function with an overoxidizing Mdh. These observations suggest that additional adaptations are required to metabolically accommodate a non-overoxidizing Mdh, which is not surprising given that MEcoli_ref_2 was evolved in the

https://doi.org/10.1038/s41467-025-65949-9

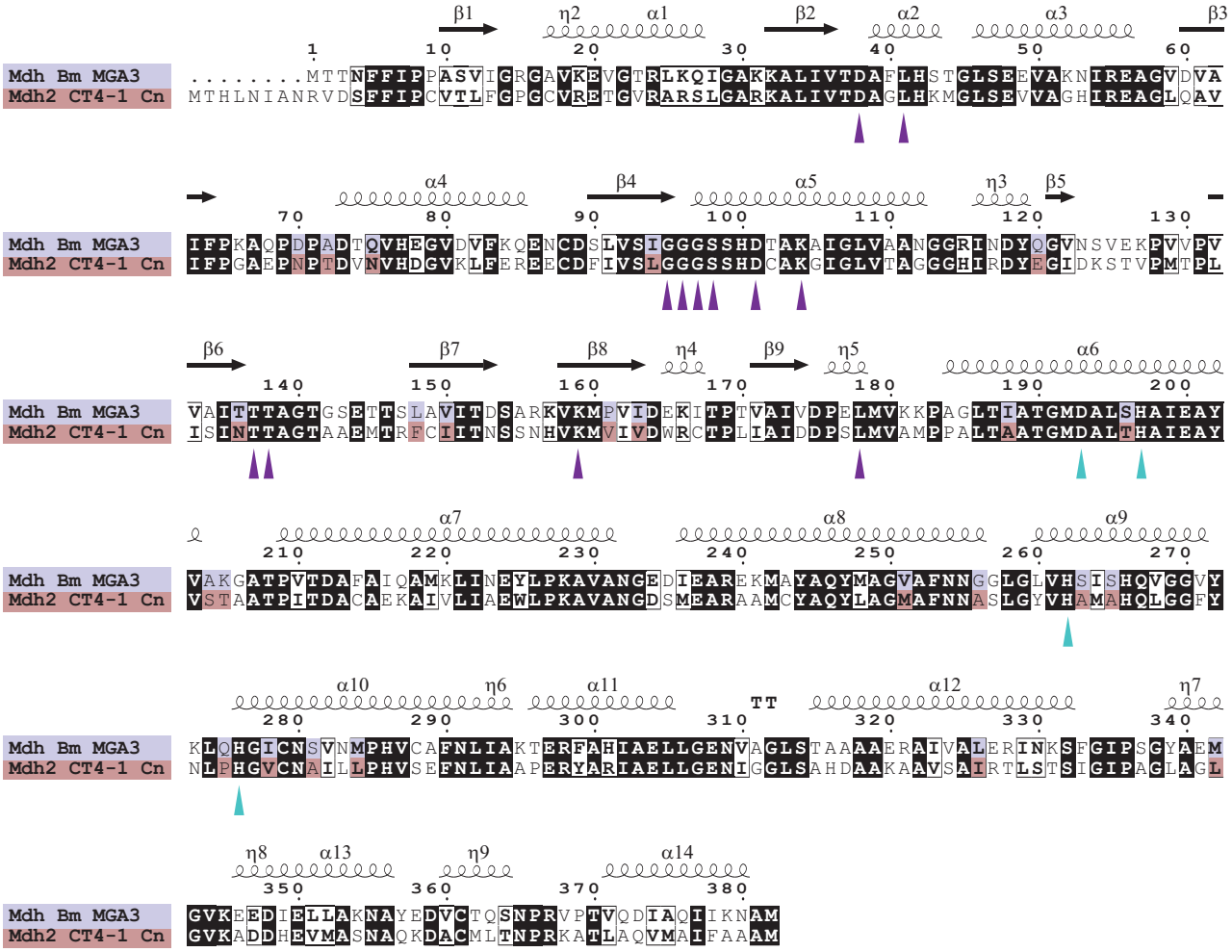

Fig. 6 | Sequence alignment of NAD-dependent methanol dehydrogenases showing conserved residues. Sequence alignment of Mdh Bm MGA3 (blue) and Mdh2 CT4-1 Cn (red), as representatives of non-overoxidizing and overoxidizing Mdh type enzymes, respectively. Residues that were found to be conserved within each respective group but differ between the two groups are highlighted in blue and red. These group-specific residues were determined by aligning all tested type III Adh enzymes tested in this study (Supplementary Fig. 13). Secondary structure information was obtained from structural predictions of Mdh2 CT4-1 Cn. Conserved NAD-binding and metal ion coordinating residues[58,60,102], are indicated by purple and blue triangles, respectively. Source data are provided as a Source Data file.

presence of an overoxidizing Mdh, potentially resulting in genomic changes affecting redox balancing, for example. Further efforts will be needed to achieve successful enzyme replacement in fully synthetic methylotrophic systems.

To nonetheless study the effect of overoxidizing versus non-overoxidizing enzymes and their impact on formate production, we introduced two of the non-overoxidizing *mdh* genes (*mdh* Bm MGA3 and *mdh* Bm PB1, respectively) along with the RuMP cycle genes *hps* and *phi* into the methanol-dependent Δ*frmA*Δ*tpiA* background. Methanol-dependent growth has the advantage that it can be readily established due to the lower biomass contribution of methanol[26]. We adapted the two strains for methanol-dependent growth as previously described for *mdh2* CT4-1 Cn (ref. 26) but only obtained a methanol-dependent strain for Mdh Bm MGA3 (for details see Supplementary Fig. 15 and Supplementary Data 5-8 and 13-20). We observed 13 times lower amounts of formate (Fig. 7a, Supplementary Data 21) for this strain than for the methanol-dependent strain expressing *mdh*2 CT4-1 Cn (Fig. 7b, Supplementary Data 3). These results demonstrate that methanol-dependent growth of *E. coli* using a non-overoxidizing, Mdh, here Mdh Bm MGA3, is possible and that formate accumulation can be significantly reduced. The replacement of Mdh also indicates that overoxidation of methanol by Mdh2 CT4-1 Cn was responsible for formate accumulation in previously described synthetic methylotrophic *E. coli* strains.

Discussion

In this work, we showed that the overoxidation of methanol to formate is a common characteristic of NAD-dependent methanol dehydrogenases. We also identified three Mdh enzymes that exclusively catalyze the oxidation of methanol to formaldehyde. The three non-overoxidizing enzymes belong to the Mdh/Mdh1-type cluster from *B. methanolicus*[44]. The genes *mdh* Bm MGA3 and *mdh* Bm PB1 are essential for methylotrophy in their native hosts[44,61,62]. They are expressed from a multi-copy endogenous plasmid, and the encoded Mdh enzymes constitute up to 22% of the proteome in the natural methylotrophic *B. methanolicus* strains MGA3 and PB1[32,63]. The gene *mdh1* Bm PB1 also belongs to this cluster but is expressed from the genome[44]. Interestingly, the genomes of *B. methanolicus* strains MGA3 and PB1 also contain genes encoding Mdh enzymes that were previously categorized as Mdh2/Mdh3-type enzymes, which we have now found to overoxidize methanol to formate. The separation of Mdh enzymes into two clusters was based on their respective amino acid sequences, which are at least 30% different[44]. Similar in vitro activity on methanol has been reported for the Mdh/Mdh1 and Mdh2/Mdh3 type

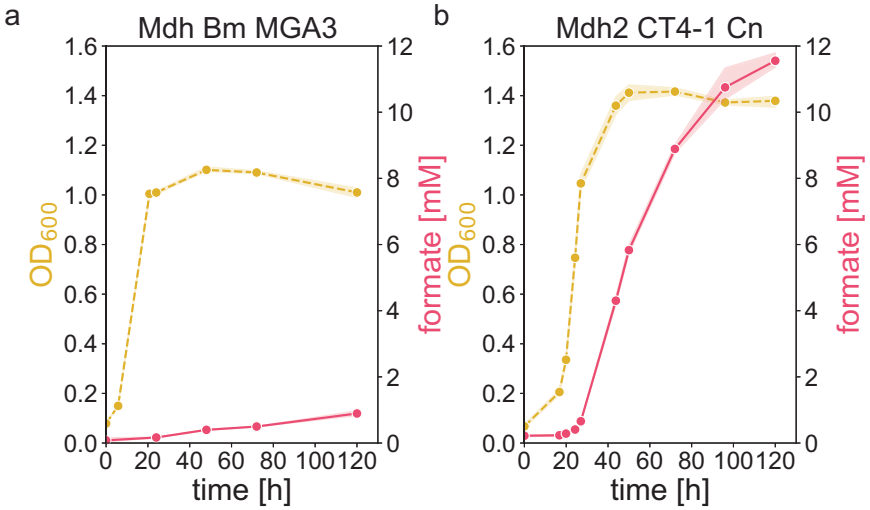

Fig. 7 | Methanol-dependent strain expressing the non-overoxidizing Mdh Bm MGA3 produces significantly less formate than the analogous strain producing an overoxidizing Mdh. Optical density and formate production of the methanol-dependent strain Δ*frmA*Δ*tpiA* expressing *hps* and *phi* and either *mdh* Bm MGA3 (**a**) or *mdh*2 CT4-1 Cn (**b**) during growth on methanol (500 mM) and pyruvate (20 mM) ($n = 3$). Pyruvate is depleted at the entry to stationary phase while methanol remains available (Supplementary Fig. 16). The mean of the data is shown as solid line and the shaded regions represent the range of the 95% confidence intervals. Source data are provided as a Source Data file.

enzymes, but the physiological relevance of having two Mdh clusters remained unclear[44,50]. The observed non-overoxidation of methanol by the Mdh/Mdh1-type cluster, in contrast to the overoxidation by the Mdh2/Mdh3-type enzymes, may hint at potential reasons for producing two distinct sets of Mdh enzymes.

B. methanolicus utilizes the RuMP cycle for growth on methanol. In this pathway, formaldehyde is assimilated by Hps through its addition to Ru5P. Consequently, the conversion of methanol by a non-overoxidizing Mdh ensures that formaldehyde is available for further assimilation rather than being removed by oxidation to formate. In contrast, the capability of the Mdh2/Mdh3 type enzymes to oxidize formaldehyde to formate suggests that their main role is not the oxidation of methanol but the detoxification of formaldehyde. Canonically, *B. methanolicus* detoxifies formaldehyde via the oxidative pentose phosphate pathway, which requires the regeneration of the one-carbon acceptor ribulose 5-phosphate (Ru5P). However, when Ru5P regeneration is ineffective, formaldehyde detoxification cannot take place. In this case, the Mdh2/Mdh3 type enzymes might serve as a backup system for the detoxification of formaldehyde, while at the same time supporting the oxidation of methanol to formaldehyde as soon as Ru5P pools have been restored. It might thus be particularly important during transition phases of changing environmental conditions with sudden up- or down shifts in methanol concentration. Whether such a system only evolved in *B. methanolicus* remains open, but so far, this is the only species in which both overoxidizing and non-overoxidizing NAD-dependent Mdh enzymes have been found.

The gram-positive methylotrophic bacterial species *Amycolatopsis methanolica* and *Mycobacterium gastri* were shown to employ *N,N'*-dimethyl-4-nitrosoaniline (NDMA)-dependent Mdh (methanol: NDMA oxidoreductase (MNO)) that is similar, but more distantly related to, NAD-dependent Mdh/Mdh1 and Mdh2/3. MNO enzymes were found to oxidize not only alcohols but also the corresponding aldehydes[64,65]. The oxidation of aldehydes by group I zinc- and NAD-dependent alcohol dehydrogenases such as horse liver alcohol dehydrogenase (HLADH) has been reported as well[66,67]. Here we showed that Mdh *Geobacillus stearothermophilus*, which belongs to group I Adhs, overoxidizes methanol to formate. In contrast to gram-positives, gram-negative methylotrophs utilize PQQ-dependent methanol dehydrogenases to oxidize methanol. PQQ-dependent ethanol dehydrogenases from *Pseudomonas* species are in fact known to overoxidize alcohols to carboxylic acids[68,69]. The in vitro oxidation of formaldehyde has also been shown for the periplasmic lanthanide-dependent Mdh XoxF from *Methylobacterium extorquens*[70,71]. It was therefore suggested that XoxF functions as both a methanol dehydrogenase and a formaldehyde dehydrogenase. However, there is evidence that XoxF does not overoxidize methanol to formate in vivo[71]. The lanthanide-dependent ethanol dehydrogenase ExaF, on the other hand, has recently been shown to oxidize formaldehyde in *M. extorquens*, suggesting the importance of PQQ-dependent Mdh enzymes as formaldehyde detoxification systems in natural methylotrophs[71,72].

To prevent the overoxidation of methanol to formate and halt the reaction at formaldehyde, a non-overoxidizing Mdh must effectively exclude formaldehyde from its active site in the presence of NAD^+. This is challenging because, in aqueous solution, formaldehyde is predominantly present as methylene glycol[46–49], which closely resembles methanol. Understanding the active site and substrate entry channel architecture of the two classes of Mdh enzymes could provide valuable insights into how these enzymes discriminate between substrates and avoid overoxidation. This would not only shed light on the molecular mechanisms underlying this process but also enhance our broader understanding of how enzymes can distinguish between structurally similar small molecules. The amino acid residues identified here (Fig. 6) might provide a starting point—together with structural investigations—to pinpoint the mechanism that prevents Mdh/Mdh1 enzyme from overoxidation. These insights might also inspire synthetic chemical approaches. In fact, aldehydes are relevant intermediates for the food and fragrance industry. The selective oxidation of alcohols to aldehydes, with or without subsequent overoxidation to carboxylic acids, is an important area of synthetic organic chemistry[73]. Efforts in this field aim to identify selective catalysts with desirable characteristics[74–77]. The relevance of Nudix hydrolases, such as *B. methanolicus* Act, for growth of methylotrophic bacteria using NAD-dependent methanol dehydrogenases also requires further investigation. While multiple studies have described the apparent activation of NAD-dependent Mdh by Nudix hydrolases in vitro[21,44,51,52,54], recent findings indicate that these enzymes function by removing the inhibitor ADP-ribose rather than providing direct activation[55]. In this study, we did not observe an effect of Act on overoxidation.

Our finding that Mdh1 and Mdh2/3 enzymes catalyze methanol oxidation to formaldehyde and formate, respectively, is important not

only to understand natural methylotrophs but also to inform the engineering of synthetic methylotrophic *E. coli* strains (or other synthetic methylotrophs) for maximal product formation. Production yields close to the theoretical maximum will be important to realize economically profitable bioprocesses from methanol by methylotrophic organisms. The production of formate by synthetic methylotrophic *E. coli* has a negative impact on the process yield as formate cannot be assimilated by *E. coli* utilizing the RuMP cycle and is lost. The engineering of an additional pathway for formate assimilation would solve this problem but would negatively affect the metabolic efficiency in general. Our work indicates that the overoxidation of methanol to formate by the NAD-dependent methanol dehydrogenase is the main origin of the observed formate production. Indeed, the replacement of the overoxidizing Mdh2 CT4-1 from *C. necator* in a formate-producing methanol-dependent strain with the non-overoxidizing Mdh from *B. methanolicus* MGA3 led to a significant reduction in formate formation. We hypothesize that this approach would also reduce the formate production by fully synthetic methylotrophic *E. coli* strains in future work. Ultimately, the generation of a synthetic methylotrophic *E. coli* strain that does not produce formate as a side product would constitute an important step towards economical bioprocesses to produce green chemicals from methanol and the establishment of a circular carbon economy.

Methods

Reagents and media

Chemicals were obtained from Sigma-Aldrich Chemie GmbH, Buchs, Switzerland unless otherwise specified. The M9 minimal medium used for bacterial cultivation consisted of the following salts (g L^{-1}): Na_2HPO_4 (6.78), KH_2PO_4 (3.0), NaCl (0.5), NH_4Cl (1.0), $CaCl_2$ (0.011), $MgSO_4{\cdot}7H_2O$ (0.493) and trace elements. Trace elements were present in the medium at the following concentrations (mg L^{-1}): $Na_2EDTA{\cdot}2H_2O$ (5.0), $MnCl_2$ (4.2), $FeSO_4{\cdot}7H_2O$ (1.0), $Co(NO_3)_2{\cdot}6H_2O$ (1.0), $ZnSO_4{\cdot}7H_2O$ (1.0), $CuSO_4{\cdot}5H_2O$ (0.1), $Na_2MoO_4{\cdot}2H_2O$ (0.1), $NiCl_2{\cdot}6H_2O$ (0.2). If indicated, antibiotics were added in the following concentrations (mg L^{-1}): ampicillin sodium (100), carbenicillin disodium (50), streptomycin sulfate (20); chloramphenicol (4.25). The chloramphenicol was dissolved in water and not in ethanol in the stock solution (850 mg L^{-1}) to avoid the presence of ethanol as additional carbon source. isopropyl-β-d-thiogalactopyranosid (IPTG) was used as inducer during methanol-dependent growth and plasmid overexpression for purification if indicated.

Primers and plasmids

Primers and plasmids used in this study are listed in Supplementary Data 22. The nucleotide sequence of the plasmids was confirmed by PCR and Sanger or Nanopore sequencing (Microsynth AG; Switzerland). The coding sequence for *mdh2* CT4-1 Cn[45] and *mdh Gs* were synthesized by Eurofins. Genes *mdh* Lx and its two mutants, *mdh* Bm C1, *adh* Sp, *mdh* Ag, *adh* Hc, *tdh* Pa, *adh* Hr, *tdh* Wc, *tdh* P, *mdh* B, were synthesized by Twist. Mdh genes from Bm MGA3 and PB1 were amplified from pSEVA424 plasmids[21]. Transfer of *mdh* genes between vectors was performed by PCR amplification and isothermal assembly utilizing the commercially available HIFI DNA Assembly mastermix (NEB). The plasmid pSEVA424 was used to express *mdh* variants for methanol-dependent growth and the overoxidation screens displayed in Fig. 3, Supplementary Fig. 6 and 8. Methanol-dependent strains in addition contained pSEVA131 for *hps*, *phi* expression. pSEVA424 and pSEVA131 backbones were isolated from the synthetic methylotrophic *E. coli* strain MEcoli_ref_2[42]. For expression, purification and the overoxidation screen displayed in Supplementary Fig. 8, a modified pET-16b expression vector (Novagen) without His_{10}-tag and its corresponding linker region was utilized. In case of the *pykF* control, the pET-16b vector still contained the His_{10}-Tag. The *mdh2* CT4-1 Cn H165N and *mdh2* CT4-1 Cn H165N F279I mutants were obtained by PCR amplification of the vector containing *mdh2* CT4-1 Cn using a mutagenic forward primer with overhang and subsequent isothermal assembly. pET21a expression plasmid containing the activator *act* Bm MGA3 (Uniprot No. I3EA59) were received from SINTEF, Norway[44,54]. pCas encoding *cas9* for CRISPR-Cas9-assisted recombineering[78] was obtained from Addgene (plasmid #62225). pTargetF_sacB was used as the vector for the sgRNA and was generated by integrating the *sacB* gene into pTargetF[78], obtained from Addgene (plasmid #62226). The *sacB* gene from pK18mob_sacB was amplified by PCR, and the product as well as pTargetF digested with XhoI and BglII (Thermo Fisher Scientific, USA). The fragments were assembled using T4 ligase (Thermo Fisher Scientific). The N20 region, which is responsible for targeting, was exchanged in pTargetF_sacB by PCR to generate pTargetF_sacB_frmRAB and pTargetF_sacB_tpiA.

Strains

The strains used in this study are listed in Supplementary Data 22. The synthetic methylotrophic *E. coli* strain MEcoli_ref_2 is able to grow on methanol as its sole carbon and energy source[42]. The methanol-dependent *E. coli* strain Δ*frmA*Δ*tpiA* expressing the RuMP cycle genes *mdh, hps* and *phi*[26] served as the ancestral strain for the ALE of MEcoli_ref_2[30]. The strains Δ*frmRAB* and Δ*frmRAB*Δ*tpiA* were generated by CRISPR/Cas engineering[78]. The exchange of *frmA* in BL21-Gold (DE3) by a kanamycin resistance cassette was achieved by the pSIM homologous recombination system[79] using the *frmA* deletion strain from the Keio collection[80] as template strain. Genomic modifications were verified by PCR and Sanger sequencing (Microsynth AG; Switzerland).

Formate production by MEcoli_ref_2 during growth on methanol in a bioreactor

Supernatant samples were derived from the bioreactor run of MEcoli_ref_2 performed in Reiter et al.[42] and were analyzed by LC-MS. See Supplementary Data 1 for a detailed overview of the bioreactor run.

L-lactic acid, itaconic acid production and formate side-production by MEcoli_ref_2 from methanol in shake flasks

Production of L-lactic acid and itaconic acid was performed as described[42]. Briefly, the cryogenic glycerol stocks of MEcoli_ref_2 + pl_lac (lactic acid production) and MEcoli_ref_2 + pl_ita (itaconic acid production) were inoculated in 20 mL volume of M9 medium supplemented with 500 mM methanol, 0.1 g L^{-1} yeast extract and chloramphenicol in baffled 100 mL shake flasks. The cultures were incubated at 37 °C, 220 revolutions per minute (r.p.m.), 25 mm throw. In the exponential growth phase, eight replicate 20 mL cultures in M9 medium containing 500 mM methanol were inoculated to an initial OD_{600} of 0.05. At $OD_{600} \approx 1.2$ (pl_lac) and $OD_{600} \approx 1.0$ (pl_ita), production was induced by transferring the cells to fresh medium containing 500 nM anhydrotetracycline (atc) (Cayman Chemical). For the transfer, the cultures were centrifuged for 7 min at 3220 g, the supernatant discarded, and the cells resuspended in fresh medium. Subsequently, the cultures were incubated in the dark at 37 °C, 180 r.p.m., 50 mm throw. For a detailed overview, see Supplementary Data 2. For supernatant sampling, 500 μL of culture were centrifuged for 1 min at 11,000 x g, 450 μL of supernatant transferred to a fresh tube and stored at −20 °C until further analysis. Formate and itaconic acid were quantified by LC-MS, L-lactic acid by a commercially available enzymatic kit.

Adaptation of methanol-dependent strains to growth without yeast extract

The methanol-dependent Δ*frmA*Δ*tpiA* and Δ*frmRAB*Δ*tpiA* strains require yeast extract as growth accelerator[26], which can be omitted after a couple of serial passages. For the adaptation of a strain to growth without yeast extract, cells were adapted in different conditions. Concentrations applied were methanol (500 mM for strains

expressing Mdh2 CT4-1 Cn; 750 mM for strains expressing Mdh Bm MGA3 or Mdh Bm PB1), 20 mM pyruvate, 0.1 g L^{-1} yeast extract in 20 mL M9 medium also containing, if indicated, Carb or Amp, Sm, 0.1 mM IPTG. 100 mL baffled shake flasks were used as vessels. The first passage was either inoculated from a cryogenic glycerol stock or an agar plate. Cultures were incubated at 37 °C using a Multitron shaker (Infors-HT) at 220 r.p.m., 25 mm throw. Once cells reached stationary phase, cultures were diluted. Passaging was repeated until growth without yeast extract was observed and the adapted culture was stored as cryogenic glycerol stock (25% glycerol) at -80 °C until further analysis. For the detailed adaptation of each strain utilized in this study, see Supplementary Fig. 15b and Supplementary Data 5-8 for Δ*frmA*Δ*tpiA* Mdh2 CT4-1 Cn; Supplementary Data 9 for Δ*frmRAB*Δ*tpiA* Mdh2 CT4-1 Cn; Supplementary Fig. 15a and Supplementary Data 13–16 for Δ*frmA*Δ*tpiA* Mdh Bm MGA3; and Supplementary Fig. 15c and Supplementary Data 17–20 for Δ*frmA*Δ*tpiA* Mdh Bm PB1.

Formate production during methanol-dependent growth

The cryogenic glycerol stock of the adapted methanol-dependent Δ*frmA*Δ*tpiA* strain expressing the RuMP cycle genes *mdh*2 CT4-1 H165N Cn, *hps* Mf, and *phi* Mf (pSEVA plasmid backbones were isolated from MEcoli_ref_2[42], see Supplementary Data 5-8 for adaptation) were streaked out on a M9 minimal medium agar plate containing 500 mM methanol, 20 mM pyruvate, Sm, Amp and incubated at 37 °C until colonies were formed. Four single colonies were inoculated in 20 mL M9 medium containing 500 mM methanol, 20 mM pyruvate, 0.1 g L^{-1} yeast extract, Amp, Sm, 0.1 mM IPTG in 100 mL baffled shake flasks and incubated at 37 °C using a Multitron shaker (Infors-HT) at 220 r.p.m., 25 mm throw. Once cells reached late exponential/stationary phase, they were diluted by pipetting the required volume of culture into fresh medium with the same composition but without yeast extract. Once cells reached exponential phase, they were diluted again for the main culture. For supernatant sampling, 500 μL of culture were centrifuged for 1 min at 11,000 x g, 450 μL of supernatant transferred to a fresh tube and stored at −20 °C until analysis by LC-MS.

For the adapted methanol-dependent strain harboring the same plasmids but containing a deletion of the entire formaldehyde detoxification pathway operon (Δ*frmRAB*Δ*tpiA*), the same procedure was followed but there was only 1 preculture and it was directly inoculated from a cryogenic glycerol stock.

For the adapted methanol-dependent Δ*frmA*Δ*tpiA* strain expressing *mdh* Bm MGA3 or *mdh*2 CT4-1 Cn together with *hps* Mf, and *phi* Mf, the same procedure was followed but the preculture originated from the seventh passage of lineage 1 of their respective adaptation to growth without yeast extract (see also Supplementary Data 5 and 13) and was passaged another five times for *mdh* Bm MGA3 or 6 times for *mdh*2 CT4-1 Cn until formate in the supernatant was quantified.

See Supplementary Data 3, 4, 10, and 21 for the detailed cultivation of each methanol-dependent strain tested for formate production in this study.

Isotopic labeling experiment to determine origin of formate during methanol-dependent growth

The preculture handling and conditions were the same as described for the adapted methanol-dependent Δ*frmA*Δ*tpiA* strain expressing the RuMP cycle genes *mdh*2 CT4-1 H165N Cn, *hps* Mf, and *phi* Mf in the previous paragraph with the following exceptions: 500 mM ^{13}C instead of ^{12}C methanol was used for the 2nd preculture and the main culture; the culture volume was 10 mL; for the passaging from the 1st to the 2nd preculture, cells were transferred by centrifugation of the required culture volume, discarding the supernatant, and solution of the cell pellet in the fresh medium. Supernatant samples were also analyzed by LC-MS. See Supplementary Data 4 for the detailed cultivation.

Heterologous expression of enzymes

E. coli BL21-Gold (DE3) cells containing the expression vector were grown in 200 mL LB medium supplemented with Carb in 2 L baffled shake flasks at 37 °C using a Multitron shaker (Infors-HT) at 220 r.p.m., 25 mm throw. At an OD_{600} of about 0.7 (mid-exponential phase) the expression was induced with 0.3 mM IPTG and the culture was incubated overnight (about 16 h) at 16 °C. The cells were harvested by centrifugation (11,000 x g, 10 min, 4 °C) and either stored at -20 °C or directly used for purification.

Purification of methanol dehydrogenases

Cell pellets were resuspended using 25 mL of buffer A (20 mM Tris, 20 mM NaCl, 2 mM DTT, pH 7.4 (adjusted with HCl)) supplemented with Roche cOmplete EDTA-free protease inhibitor cocktail (Sigma-Aldrich Chemie GmbH, Buchs, Switzerland). Cell lysis was performed by sonication (6 mm sonication probe, amplitude 30, process time 4 min, impulse time 5 s followed by 25 s cooling, Q700 sonicator (Qsonica LLC, U.S.A)) and cell debris was removed by centrifugation (18,000 x g, 40 min, 4 °C).

As first chromatographic step to obtain untagged Mdh2 CT4-1 Cn and Mdh Bm MGA3, the lysate was purified using a 1 mL HiTrap Q HP (Cytiva, Marlborough, Massachusetts, U.S.A.) anion exchange column by applying a linear gradient of buffer A to buffer B (20 mM Tris, 1 M NaCl, 2 mM DTT, pH 7.4 (adjusted with HCl)). The gradient was run at 1 mL min^{-1} from 0% B to 60% B in 30 min. The collected fractions were analyzed by SDS-PAGE, and fractions containing methanol dehydrogenase were pooled and concentrated using 50 kDa centrifugal filter units (Amicon, Merck).

As a next step, the sample was purified by size exclusion chromatography using Superdex 200 Increase 10/300 GL column run with buffer C (50 mM sodium phosphate buffer (37.7 mM sodium phosphate dibasic, 12.3 mM sodium phosphate monobasic), 150 mM NaCl, 5 mM $MgSO_4$, pH 7.4 (adjusted with NaOH)). The methanol dehydrogenase-containing fractions were analyzed by SDS-PAGE, collected and concentrated. Protein concentration was determined by absorption measurement at 280 nm using a NanoDrop spectrophotometer and the calculated extinction coefficient of 21,430 M^{-1} cm^{-1} (Mdh2 CT4-1 Cn) or 11,920 M^{-1} cm^{-1} (Mdh Bm MGA3), respectively (Expasy ProtParam). The enzymes were stored at 4 °C.

Purification of activator protein (Act)

His_6-tagged Act Bm MGA3 was purified by resuspending cell pellets in 20 mL buffer A (50 mM sodium phosphate monobasic, 300 mM NaCl, 20 mM imidazole, 2 mM DTT, pH 8 (adjusted with NaOH)) supplemented with Roche cOmplete EDTA-free protease inhibitor. Cell lysis and clearance of cell debris was performed as described above.

Act was isolated from the lysate by affinity chromatography using a 1 mL HisTrap HP (Cytiva, Marlborough, Massachusetts, U.S.A.) column and applying a linear gradient of buffer A to buffer B (50 mM sodium phosphate monobasic, 300 mM NaCl, 500 mM imidazole, 2 mM DTT, pH 8 (adjusted with NaOH)). The gradient was run at 1 mL min^{-1} from 0% B to 100% B in 25 min. Fractions containing Act were pooled and analyzed by SDS-PAGE. Buffer was exchanged to reaction buffer (50 mM sodium phosphate buffer (37.7 mM sodium phosphate dibasic, 12.3 mM sodium phosphate monobasic), 5 mM $MgSO_4$, pH 7.4 (adjusted with NaOH)) by repeated concentration using 10 kDa centrifugal filter units (Amicon, Merck) and refills with reaction buffer until a dilution factor of at least 30,000 was achieved. Protein concentration was determined by absorption measurement at 280 nm using a NanoDrop spectrophotometer and the calculated extinction coefficient of 14,440 M^{-1} cm^{-1} (Expasy ProtParam). The enzyme was stored at 4 °C.

In vitro enzyme assays

Activity assays were performed in cuvettes using a Cary 50 Bio UV-Visible spectrophotometer (Varian, Steinhausen, Switzerland). Methanol dehydrogenase activity was assayed in reaction buffer (buffer C) supplemented with 12.3 µM Mdh2 CT4-1 Cn or 12.5 µM Mdh Bm MGA3 and 5 mM NAD^+ at 37 °C. For the in vitro measurements involving Act (Supplementary Fig. 12), 3.1 µM Mdh Bm MGA3 and, if indicated, 2.3 µM activator protein (Act) was added. Assays were started by adding preheated (10 min) methanol or formaldehyde (10 µL) to preheated reaction buffer containing Mdh and NAD^+, followed by mixing by pipetting up and down. The reaction was monitored by measuring the increase in NADH at 340 nm and the NADH concentration was calculated from its extinction coefficient ($\varepsilon_{340} = 6220\ M^{-1}\ cm^{-1}$). The rate of NADH formation from methanol or formaldehyde in vitro for 10, 20, 50, 100, and 500 mM methanol and formaldehyde as initial concentrations represent the maximal slope of NADH formation over a period of at least 5 s in the first 40 s of recording for Mdh2 CT4-1 Cn and 10 s in the first 300 s of recording for Mdh Bm MGA3. To investigate the equilibrium states of the in vitro reactions (Fig. 5a), the assay was performed using a microplate reader (BioTek Synergy H1, Agilent Technologies) and 25 µM Mdh2 CT4-1 Cn or 25 µM Mdh Bm MGA3. ^{13}C methanol was used in the experiment to enable the quantification of ^{13}C formate by *1D* ^{13}C NMR. The equilibrium concentrations of formaldehyde, formate, and NADH were determined by the following methodologies: Formaldehyde was quantified by Nash assay. Formate was quantified by NMR. NADH was quantified by the absorbance of the reaction solution at 340 nm, using a standard curve obtained with a commercially available NADH standard (Sigma).

Formate production of the Δ*frmRAB* strains harboring plasmids encoding different NAD-dependent methanol dehydrogenases

Cryogenic glycerol stocks of the BW25113 Δ*frmRAB* strains harboring an empty pSEVA424 plasmid backbone isolated from MEcoli_ref_2 or expressing different NAD-dependent Mdh enzymes were inoculated into 4 mL LB cultures in 14 mL plastic culture tubes and grown to stationary phase at 37 °C using a Multitron shaker (Infors-HT) at 220 r.p.m., 25 mm throw. Triplicate cultures were inoculated in 20 mL M9 medium containing 20 mM pyruvate, 0.1 mM IPTG and 500 mM methanol to a starting OD_{600} of 0.05 by direct transfer of the respective volume of LB preculture. 100 mL baffled shake flasks were used as vessels. Culture supernatants were sampled at 5, 22, 46, and 69 hours after inoculation. Samples for the quantification of formate by HPLC were generated by centrifugation of 500 µL of cell culture at 11,000 x g, 4 °C for 3 min. Next, 400 µL of the supernatant was carefully aspirated and subsequently stored in screw-cap tubes at -20 °C until analysis by HPLC. Data from this method are shown in Fig. 3a and Supplementary Fig. 6. See Supplementary Data 11 for culture density and formate concentration of individual replicates over time.

Plasmids were transformed into BL21-Gold (DE3) Δ*frmA*::kan and BW25113 Δ*frmRAB* by electroporation. Three single colonies were inoculated into 3 mL LB cultures in 24-deep well plates and grown to stationary phase at 37 °C using a Multitron shaker (Infors-HT) at 220 r.p.m., 25 mm throw. Triplicate cultures were inoculated in 20 mL M9 medium containing 20 mM pyruvate, 0.1 mM IPTG and 500 mM methanol to a starting OD_{600} of 0.05 by direct transfer of the respective volume of LB preculture. 100 mL baffled shake flasks were used as vessels. Culture supernatants were sampled 0, 24, 48, 72, and 144 hours by filtration of 500 µL culture through 96-well filter plates (Cytiva, AcroPrep). Supernatants were stored in 96-well plates at -20 °C until analysis by NMR. Data from this method are shown in Supplementary Fig. 8. See Supplementary Data 12 for culture density and formate concentration of individual replicates over time.

Quantification of L-lactic acid

L-lactic acid in the culture supernatant was quantified by a commercially available enzyme kit (L-Lactic Acid (L-Lactate) Assay Kit, K-LATE, Megazyme) according to the manufacturer protocol.

Quantification of formate, itaconic acid, and pyruvate by LC-MS

Organic acids in the culture supernatant were derivatized together with an internal standard as described[81]. Briefly, 200 µM sodium propionate was used as internal standard for the simultaneous quantification of formate and itaconic acid, and for the determination of $^{12}C/^{13}C$ formate ratio in the isotopic tracer experiment displayed in Fig. 1c. When only formate was quantified, 1 mM of isotopically labeled ^{13}C formate (Cambridge Isotope Laboratories) was used as internal standard. For the quantification of pyruvate, no internal standard was used.

Samples were diluted 20-fold in 50% (v/v) acetonitrile and 34 mM 3-nitrophenylhydrazine (3-NPH) and 21 mM N-(3-dimethylaminopropyl)-N′-ethylcarbodiimide (EDC) were added. Samples were incubated at 40 °C with continuous shaking for 1 h to facilitate the derivatization reaction. The reaction was quenched by the addition of 0.02 % (v/v) trifluoroacetic acid (TFA) and diluted 10-fold in 50% (v/v) acetonitrile. For the derivatization of samples for pyruvate quantification, the protocol was slightly adapted: 33 mM 3-NPH and 20 mM EDC were used, 1 % pyridine was added, incubation was 30 min, 0.014 % (v/v) TFA was added. Derivatized samples were analyzed using UPLC (UPLC Ultimate 3000, Thermo Fisher Scientific) with a C18 column with isobutyl side chains and tetramethylsilane end capping (Kinetex Core-Shell Technology XB-C18: 2.1 × 50 mm, 1.7 µm particle size, 100 Å pore size, Phenomenex) coupled to a hybrid quadrupole-orbitrap mass spectrometer (Q Exactive Plus, Thermo Fisher Scientific). Solvents were 0.1% (v/v) formic acid in ultrapure water (solvent A) and in acetonitrile (solvent B)[81]. For metabolite separation, the following gradient was used at a constant flow rate of 500 µL min^{-1}: 98% solvent A linearly decreased to 5% in 3 min, then held at 5% A for 2 min, then linearly increased to 98% in 0.3 min and held at 98% for a final 2 min. Fourier-transform MS was performed in negative mode with a spray voltage of −3.0 kV, a capillary temperature of 275 °C, an S-lens radiofrequency level of 50, an auxiliary gas flow rate of 20 a.u. and an auxiliary gas heater temperature of 350 °C. Mass spectra were recorded as centroids at a resolution of 35,000 at an *m/z* of 200 with a mass range of 150–1000 *m/z* and a scan rate of ~4 Hz in full scan mode. 2 µL of sample were injected. Organic acids were quantified using pure formic acid (Fisher Scientific) or itaconic acid (Chemie Brunschwig) as external standards diluted in M9 medium derivatized with internal standard as described above. LC/MS results were analyzed using the eMZed framework (emzed.ethz.ch)[82]. Metabolite peaks were extracted via a targeted approach using the external standard to define retention time–*m/z* peak windows applying an *m/z* tolerance of 10 ppm. Integration was performed using trapezoid integration. The ^{13}C formate internal standard was corrected for the natural abundance of labeled formate in the sample and of labeled derivatization reagent.

Formate quantification by HPLC

Formate in the supernatant of the cultures for the methanol dehydrogenase screen for overoxidation of methanol was quantified via UPLC (UPLC Ultimate 3000) equipped with a Rezex ROA UPLC column (Rezex ROA-Organic Acid H+ (8%): 300 × 7.8 mm; Phenomenex) coupled to a variable wavelength detector VWD-3400 (Thermo Fisher Scientific) by monitoring the absorbance at 210 nm. 2.5 mM sulfuric acid in ultrapure water was used as solvent at an isocratic gradient and a flow rate of 600 µL min^{-1}. 20 µL of sample was injected. Peaks were identified and the peak areas were quantified using Chromeleon 7 software (Thermo Fisher Scientific) based on an external standard curve of pure formic acid (Fisher Scientific) utilizing a standard dilution series in ultrapure water. Prior to injection, samples were diluted

1:1 (v/v) in ultrapure water and standards 1:1 (v/v) in M9 medium to exclude matrix effects.

Formate quantification by NMR

A total of 90 µL of reaction mixture were mixed with 20 µL D_2O (99.8 %, Merck, 617385-1-107KG) containing 10 mM DSS-D6 (98 %, CIL DLM-8206-1). 80 µL of 20 mM sodium acetate buffer and 10 µL of 1 M acetic acid were added to acidify the sample. This mixture resulted in a final DSS proton concentration of 1000 µM. The prepared solutions were transferred to 3 mm NMR tubes, suitable for use with the SampleJet system (Z168406, Bruker Inc.).

NMR data were acquired at 298.0 K (Fig. 5) or 289.0 K (Supplementary Fig. 8) at a 600 MHz Bruker AVIII Avance HD NMR spectrometer equipped with a CP-QCI-1H/19F-13C/15N-2H 05 Z cryoprobe. The system included a SampleJet (Bruker Inc.) sample handling robot for automation, with the samples stored at 278 K between the experiments.

The following 1D ^{1}H method was used to obtain results shown in Supplementary Fig. 8. The experiments were acquired with 65536 complex data points and 64 transients. The pre-scan relaxation delay was set to 4.0 s. The solvent signal was suppressed by applying pre-saturation during the pre-scan delay and by applying a short (10 ms) NOE mixing period followed by a z-gradient before the final π/2 pulse. Data were zero-filled to 131,072 points, and a squared cosine window function was applied. The resulting spectra were baseline-corrected before peak integration. Peak integrals of metabolites were normalized to the integral of DSS at 0 ppm for concentration determination.

The following 1D ^{13}C method was used to obtain results shown in Fig. 5. The experiments were acquired with 53,056 complex data points and 6,144 transients. The pre-scan relaxation delay was set to 2.0 s. The carrier frequency was set to 97 ppm and the spectral width to 251 ppm. The ^{1}H channel was saturated during the pre-scan delay to enhance the ^{13}C signal due to heteronuclear nuclear Overhauser enhancement. For ^{1}H broadband decoupling during the acquisition and ^{1}H saturation during the pre-scan delay, the WALTZ-65[83,84] scheme was applied. Data were zero-filled to 131,072 points, and a squared cosine window function was applied. The resulting spectra were baseline-corrected before peak integration.

Data acquisition and processing were performed using TopSpin 3.6 (Bruker, Inc.). Formate was quantified using pure formic acid (Fisher Scientific) as external standard diluted in M9 medium.

Formaldehyde quantification by Nash assay

To quantify the formaldehyde in samples from the in vitro assays, 20 µL sample (collected at equilibrium, after 180 min (see Fig. 5a)) was taken from the assay mixture and mixed with 20 µL Nash reagent (2 M ammonium acetate, 0.05 M acetic acid, 0.02 M acetylacetone)[85]. Following an incubation of 40 min at 37 °C, absorbance at 412 nm was measured using a microplate reader (BioTek Synergy H1, Agilent Technologies). Formaldehyde concentrations were calculated with a standard curve utilizing an external formaldehyde standard.

Methanol quantification by gas chromatography

Methanol in the stationary phase of the methanol-dependent cultures was quantified using GC (GC 6850) equipped with a 7683B Series injector coupled to an FID. A DB-WAX column (15 m × 0.32 mm × 0.50 µm; Agilent Technologies) was used for metabolite separation with helium as the carrier gas at a column flow rate of 2.1 mL min^{-1}. The following temperature gradient was applied: 35 °C for 0.5 min, 1.625 min from 35 to 230 °C, 3 min at 230 °C, 1.625 min to 90 °C and then 0.5 min at 90 °C. For each sample, 0.5 µL was injected. The split ratio was 10.0 and the detector temperature was 270 °C. Peaks were confirmed using standards. For the measurements, the samples were diluted 1:1 (v:v) with 500 mM 1-butanol in ultrapure water and further diluted 1:50 (v:v) in ultrapure water. 1-butanol was used as the internal standard to correct for technical fluctuations.

Phylogenetic analysis

To obtain the phylogenetic results shown in Fig. 3b, the enzyme sequences with the following Uniprot identifiers were aligned: Mdh Bm MGA3, Q6TV41; Mdh2 Bm MGA3, I3E2P9; Mdh3 Bm MGA3, I3E949; Mdh Bm PB1, I3DTP7; Mdh1 Bm PB1, I3DX19; Mdh2 Bm PB1, I3DVX6; Mdh2 Cn WT F8GNE5 (the variant CT4-1 used in this study is A26V, A31V, A169V compared to the WT[45]); Mdh Lx, A0A0K9F7R7; Mdh Gs, P42327. The sequence alignment was performed using MUSCLE in the EMBL-EBI Job Dispatcher sequence analysis tools framework web tool[86] and the phylogenetic tree was visualized by ETE3[87].

To generate the phylogenetic results shown in Supplementary Fig. 7, 1000 protein sequences related to the Mdh Bm MGA3 were obtained by a BLASTp search over the non-redundant protein sequences (nr) database. Experimentally tested sequences that were not listed in the BLAST results were added and a multisequence alignment performed using MAFFT[88]. Aligned protein sequences were trimmed using Jalview[89]. The maximum likelihood tree was constructed with IQ-TREE[90] using the best-fit model. Node support for the phylogenetic tree was evaluated by calculating 1,000 bootstrap replicates using ultrafast bootstrap approximation. TreeViewer was used for visualization and annotation of the phylogenetic tree[91].

Sequence analysis by MSA

MSA of the protein sequences was performed using the EMBL-EBI Job Dispatcher sequence analysis tool (Clustal Omega)[86,92,93]. The default parameters for MSA were applied, except for the order which was changed to "input". The alignment was visualized with the use of ENDscript (https://endscript.ibcp.fr)[94]. For secondary structure depiction, the structure predicted for Mdh2 CT4-1 Cn (AlphaFold 3, AlphaFold Server[95]) was selected. Annotation of conserved residues was performed in Adobe Illustrator 2025 (Adobe Inc.) software (Version 29.4).

Structural predictions

Structures of Mdh2 CT4-1 Cn and Mdh Bm MGA3 were predicted using AlphaFold 3 (AlphaFold Server)[95]. The structures were analyzed and visualized in PyMOL Molecular Graphics System, Version 3.0.4 Schrödinger, LLC.

Calculation of equilibrium concentrations

For a methanol overoxidizing Mdh, the oxidation of methanol to formaldehyde and of formaldehyde to formate was considered, while for a non-overoxidizing Mdh only the methanol to formaldehyde oxidation was considered in the calculation. Estimated $\Delta_rG'°$ were derived from the eQuilibrator web tool[96–100] for the conditions present in the in vitro assays (pH = 7.4, pMg = 2.3, ionic strength = 0.15 M) and are 32 kJ/mol and −49.6 kJ/mol. The initial concentration of methanol is 500 mM and of NAD^+ 5 mM. Equilibrium concentrations of methanol [MeOH], formaldehyde [FALDH], formate [FA], [NAD^+] and [NADH] were derived from the following non-linear equation system for the overoxidizing reaction:

$$K_1 = \frac{[\mathrm{FALDH}]^*[\mathrm{NADH}]}{[\mathrm{MeOH}]^*[\mathrm{NAD}^+]} \quad (1)$$

$$K_2 = \frac{[\mathrm{FA}]^*[\mathrm{NADH}]}{[\mathrm{FALDH}]^*[\mathrm{NAD}^+]} \quad (2)$$

$$500 = [\mathrm{MeOH}]_0 \quad (3)$$

$$[MeOH]_0 = [MeOH] + [FALDH] + [FA] \quad (4)$$

$$[NADH] = [FALDH] + 2*[FA] \quad (5)$$

$$5 = [NAD^+]_0 \quad (6)$$

$$[NAD^+]_0 = [NAD^+] + [NADH] \quad (7)$$

For the non-overoxidizing reaction, the following non-linear equation system was solved using Eqs. 1, 3, 6 and 7 as well as:

$$[MeOH]_0 = [MeOH] + [FALDH] \quad (8)$$

$$[NADH] = [FALDH] \quad (9)$$

Reporting summary

Further information on research design is available in the Nature Portfolio Reporting Summary linked to this article.

Data availability

All relevant data supporting the findings of this work are provided within the paper and in its Supplementary Information files. Accession numbers of all enzymes tested are listed in Supplementary Data 22. Source data are provided with this paper.

References

1. Calvin, K. et al. IPCC, 2023: Climate Change 2023: Synthesis Report. Contribution of Working Groups I, II and III to the Sixth Assessment Report of the Intergovernmental Panel on Climate Change [Core Writing Team, H. Lee and J. Romero (Eds.)]. IPCC, Geneva, Switzerland. https://www.ipcc.ch/report/ar6/syr/ (IPCC, 2023).
2. Bachmann, M. et al. Towards circular plastics within planetary boundaries. *Nat. Sustain.* **6**, 599–610 (2023).
3. Tickner, J., Geiser, K. & Baima, S. Transitioning the chemical industry: the case for addressing the climate, toxics, and plastics crises. *Environ. Sci. Policy Sustain. Dev.* **63**, 4–15 (2021).
4. Gabrielli, P. et al. Net-zero emissions chemical industry in a world of limited resources. *One Earth* **6**, 682–704 (2023).
5. Kang, S. Innovation outlook: renewable methanol. (International Renewable Energy Agency, 2021).
6. Anthony, C. The Biochemistry of Methylotrophs. (Academic Press, 1982).
7. Motoyama, H., Yano, H., Terasaki, Y. & Anazawa, H. Over-production of L-lysine from methanol by *Methylobacillus glycogenes* derivatives carrying a plasmid with a mutated *dap*Agene. *Appl. Environ. Microbiol.* **67**, 3064–3070 (2001).
8. Gunji, Y. & Yasueda, H. Enhancement of L-lysine production in methylotroph *Methylophilus methylotrophus* by introducing a mutant LysE exporter. *J. Biotechnol.* **127**, 1–13 (2006).
9. Liang, W.-F. et al. Biosensor-assisted transcriptional regulator engineering for *Methylobacterium extorquens* AM1 to improve mevalonate synthesis by increasing the acetyl-CoA supply. *Metab. Eng.* **39**, 159–168 (2017).
10. Guo, F. et al. Metabolic engineering of *Pichia pastoris* for malic acid production from methanol. *Biotechnol. Bioeng.* **118**, 357–371 (2021).
11. Dietz, K. et al. A novel engineered strain of *Methylorubrum extorquens* for methylotrophic production of glycolic acid. *Microb. Cell Factories* **23**, 344 (2024).
12. Hurt, A., Bibik, J. D., Martinez-Gomez, N. C. & Hamberger, B. Engineering terpene production pathways in *Methylobacterium extorquens* AM1. *Microorganisms* **12**, 500 (2024).
13. Severinsen, M. M., Bachleitner, S., Modenese, V., Ata, Ö. & Mattanovich, D. Efficient production of itaconic acid from the single-carbon substrate methanol with engineered *Komagataella phaffii*. *Biotechnol. Biofuels Bioprod.* **17**, 98 (2024).
14. Àvila-Cabré, S., Pérez-Trujillo, M., Albiol, J. & Ferrer, P. Engineering the synthetic β-alanine pathway in *Komagataella phaffii* for conversion of methanol into 3-hydroxypropionic acid. *Microb. Cell Factories* **22**, 237 (2023).
15. Li, J. et al. Engineering yeast for high-level production of β-farnesene from sole methanol. *Metab. Eng.* **85**, 194–200 (2024).
16. Wu, X. et al. Efficient bioproduction of 3-hydroxypropionic acid from methanol by a synthetic yeast cell factory. *ACS Sustain. Chem. Eng.* **11**, 6445–6453 (2023).
17. Yu, W., Gao, J., Yao, L. & Zhou, Y. J. Bioconversion of methanol to 3-hydroxypropionate by engineering *Ogataea polymorpha*. *Chin. J. Catal.* **46**, 84–90 (2023).
18. Tang, H. et al. Metabolic engineering of yeast for the production of carbohydrate-derived foods and chemicals from C1–3 molecules. *Nat. Catal.* **7**, 21–34 (2024).
19. Schrader, J. et al. Methanol-based industrial biotechnology: current status and future perspectives of methylotrophic bacteria. *Trends Biotechnol.* **27**, 107–115 (2009).
20. Antoniewicz, M. R. Synthetic methylotrophy: strategies to assimilate methanol for growth and chemicals production. *Curr. Opin. Biotechnol.* **59**, 165–174 (2019).
21. Müller, J. E. N. et al. Engineering *Escherichia coli* for methanol conversion. *Metab. Eng.* **28**, 190–201 (2015).
22. Wang, X. et al. Biological conversion of methanol by evolved *Escherichia coli* carrying a linear methanol assimilation pathway. *Bioresour. Bioprocess.* **4**, 41 (2017).
23. Meyer, F. et al. Methanol-essential growth of *Escherichia coli*. *Nat. Commun.* **9**, 1508 (2018).
24. Chen, C.-T. et al. Synthetic methanol auxotrophy of *Escherichia coli* for methanol-dependent growth and production. *Metab. Eng.* **49**, 257–266 (2018).
25. Bennett, R. K. et al. Engineering *Escherichia coli* for methanol-dependent growth on glucose for metabolite production. *Metab. Eng.* **60**, 45–55 (2020).
26. Keller, P. et al. Methanol-dependent *Escherichia coli* strains with a complete ribulose monophosphate cycle. *Nat. Commun.* **11**, 5403 (2020).
27. De Simone, A. et al. Mixing and matching methylotrophic enzymes to design a novel methanol utilization pathway in *E. coli*. *Metab. Eng.* **61**, 315–325 (2020).
28. Kim, S. et al. Growth of *E. coli* on formate and methanol via the reductive glycine pathway. *Nat. Chem. Biol.* **16**, 538–545 (2020).
29. Chen, F. Y.-H., Jung, H.-W., Tsuei, C.-Y. & Liao, J. C. Converting *Escherichia coli* to a synthetic methylotroph growing solely on methanol. *Cell* **182**, 933–946.e14 (2020).
30. Keller, P. et al. Generation of an *Escherichia coli* strain growing on methanol via the ribulose monophosphate cycle. *Nat. Commun.* **13**, 5243 (2022).
31. Meng, X. et al. A synthetic methylotroph achieves accelerated cell growth by alleviating transcription-replication conflicts. *Nat. Commun.* **16**, 31 (2025).
32. Arfman, N. et al. Methanol metabolism in thermotolerant methylotrophic *Bacillus* strains involving a novel catabolic NAD-dependent methanol dehydrogenase as a key enzyme. *Arch. Microbiol.* **152**, 280–288 (1989).
33. Yu, H. & Liao, J. C. A modified serine cycle in *Escherichia coli* coverts methanol and CO_2 to two-carbon compounds. *Nat. Commun.* **9**, 3992 (2018).

34. Woolston, B. M., King, J. R., Reiter, M., Van Hove, B. & Stephanopoulos, G. Improving formaldehyde consumption drives methanol assimilation in engineered *E. coli*. *Nat. Commun.* **9**, 2387 (2018).
35. Har, J. R. G., Agee, A., Bennett, R. K., Papoutsakis, E. T. & Antoniewicz, M. R. Adaptive laboratory evolution of methylotrophic *Escherichia coli* enables synthesis of all amino acids from methanol-derived carbon. *Appl. Microbiol. Biotechnol.* **105**, 869–876 (2021).
36. Whitaker, W. B. et al. Engineering the biological conversion of methanol to specialty chemicals in *Escherichia coli*. *Metab. Eng.* **39**, 49–59 (2017).
37. Bennett, R. K., Gonzalez, J. E., Whitaker, W. B., Antoniewicz, M. R. & Papoutsakis, E. T. Expression of heterologous non-oxidative pentose phosphate pathway from *Bacillus methanolicus* and phosphoglucose isomerase deletion improves methanol assimilation and metabolite production by a synthetic *Escherichia coli* methylotroph. *Metab. Eng.* **45**, 75–85 (2018).
38. Rohlhill, J., Gerald Har, J. R., Antoniewicz, M. R. & Papoutsakis, E. T. Improving synthetic methylotrophy via dynamic formaldehyde regulation of pentose phosphate pathway genes and redox perturbation. *Metab. Eng.* **57**, 247–255 (2020).
39. Lee, J.-Y. et al. Discovery and biochemical characterization of a methanol dehydrogenase from *Lysinibacillus xylanilyticus*. *Front. Bioeng. Biotechnol.* **8**, 67 (2020).
40. Le, T.-K. et al. Biosensor-based directed evolution of methanol dehydrogenase from *Lysinibacillus xylanilyticus*. *Int. J. Mol. Sci.* **22**, 1471 (2021).
41. Price, J. V., Chen, L., Whitaker, W. B., Papoutsakis, E. & Chen, W. Scaffoldless engineered enzyme assembly for enhanced methanol utilization. *Proc. Natl Acad. Sci.* **113**, 12691–12696 (2016).
42. Reiter, M. A. et al. A synthetic methylotrophic *Escherichia coli* as a chassis for bioproduction from methanol. *Nat. Catal.* **7**, 560–573 (2024).
43. Nieh, L.-Y. et al. Evolutionary engineering of methylotrophic *E. coli* enables fast growth on methanol. *Nat. Commun.* **15**, 8840 (2024).
44. Krog, A. et al. Methylotrophic *Bacillus methanolicus* encodes two chromosomal and one plasmid born NAD+ dependent methanol dehydrogenase paralogs with different catalytic and biochemical properties. *PLoS ONE* **8**, e59188 (2013).
45. Wu, T.-Y. et al. Characterization and evolution of an activator-independent methanol dehydrogenase from *Cupriavidus necator* N-1. *Appl. Microbiol. Biotechnol.* **100**, 4969–4983 (2016).
46. Rivlin, M., Eliav, U. & Navon, G. NMR Studies of the equilibria and reaction rates in aqueous solutions of formaldehyde. *J. Phys. Chem. B* **119**, 4479–4487 (2015).
47. Hasse, H. & Maurer, G. Kinetics of the poly(oxymethylene) glycol formation in aqueous formaldehyde solutions. *Ind. Eng. Chem. Res.* **30**, 2195–2200 (1991).
48. Hahnenstein, I., Albert, M., Hasse, H., Kreiter, C. G. & Maurer, G. NMR spectroscopic and densimetric study of reaction kinetics of formaldehyde polymer formation in water, deuterium oxide, and methanol. *Ind. Eng. Chem. Res.* **34**, 440–450 (1995).
49. Gaca, K. Z., Parkinson, J. A., Lue, L. & Sefcik, J. Equilibrium speciation in moderately concentrated formaldehyde–methanol–water solutions investigated using ^{13}C and ^{1}H nuclear magnetic resonance spectroscopy. *Ind. Eng. Chem. Res.* **53**, 9262–9271 (2014).
50. Müller, J. E. N., Heggeset, T. M. B., Wendisch, V. F., Vorholt, J. A. & Brautaset, T. Methylotrophy in the thermophilic *Bacillus methanolicus*, basic insights and application for commodity production from methanol. *Appl. Microbiol. Biotechnol.* **99**, 535–551 (2015).
51. Arfman, N. et al. Properties of an NAD(H)-containing methanol dehydrogenase and its activator protein from *Bacillus methanolicus*. *Eur. J. Biochem.* **244**, 426–433 (1997).
52. Arfman, N., Van Beeumen, J., De Vries, G. E., Harder, W. & Dijkhuizen, L. Purification and characterization of an activator protein for methanol dehydrogenase from thermotolerant *Bacillus* spp. *J. Biol. Chem.* **266**, 3955–3960 (1991).
53. Vonck, J. et al. Electron microscopic analysis and biochemical characterization of a novel methanol dehydrogenase from the thermotolerant *Bacillus* sp. C1. *J. Biol. Chem.* **266**, 3949–3954 (1991).
54. Ochsner, A. M., Müller, J. E. N., Mora, C. A. & Vorholt, J. A. In vitro activation of NAD-dependent alcohol dehydrogenases by Nudix hydrolases is more widespread than assumed. *FEBS Lett.* **588**, 2993–2999 (2014).
55. Ma, B.-D., Li, J.-Y., Xu, J.-H., Yu, T. & Kong, X.-D. ADP-ribose is a competitive inhibitor of methanol dehydrogenases from *Bacillus methanolicus*. *J. Biol. Chem.* **301**, 110599 (2025).
56. Ruzheinikov, S. N. et al. Glycerol dehydrogenase: structure, specificity, and mechanism of a family III polyol dehydrogenase. *Structure* **9**, 789–802 (2001).
57. Schwarzenbacher, R. et al. Crystal structure of an iron-containing 1,3-propanediol dehydrogenase (TM0920) from *Thermotoga maritima* at 1.3Å resolution. *Proteins Struct. Funct. Bioinforma.* **54**, 174–177 (2004).
58. Montella, C. et al. Crystal structure of an iron-dependent group III dehydrogenase that interconverts l -lactaldehyde and l -1,2-propanediol in *Escherichia coli*. *J. Bacteriol.* **187**, 4957–4966 (2005).
59. Marçal, D., Rêgo, A. T., Carrondo, M. A. & Enguita, F. J. 1,3-propanediol dehydrogenase from *Klebsiella pneumoniae*: decameric quaternary structure and possible subunit cooperativity. *J. Bacteriol.* **191**, 1143–1151 (2009).
60. Moon, J.-H. et al. Structures of iron-dependent alcohol dehydrogenase 2 from *Zymomonas mobilis* ZM4 with and without NAD + cofactor. *J. Mol. Biol.* **407**, 413–424 (2011).
61. Brautaset, T. et al. Plasmid-dependent methylotrophy in thermotolerant *Bacillus methanolicus*. *J. Bacteriol.* **186**, 1229–1238 (2004).
62. Brautaset, T., Jakobsen, Ø.M., Josefsen, K. D., Flickinger, M. C. & Ellingsen, T. E. *Bacillus methanolicus*: a candidate for industrial production of amino acids from methanol at 50 °C. *Appl. Microbiol. Biotechnol.* **74**, 22–34 (2007).
63. Müller, J. E. N. N. et al. Proteomic analysis of the thermophilic methylotroph *Bacillus methanolicus* MGA3. *Proteomics* **14**, 725–737 (2014).
64. Bystrykh, L. V. et al. Formaldehyde dismutase activities in Gram-positive bacteria oxidizing methanol. *J. Gen. Microbiol.* **139**, 1979–1985 (1993).
65. Bystrykh, L. V., Govorukhina, N. I., Dijkhuizen, L. & Duine, J. A. Tetrazolium-dye-linked alcohol dehydrogenase of the methylotrophic actinomycete *Amycolatopsis methanolica* is a three-component complex. *Eur. J. Biochem.* **247**, 280–287 (1997).
66. Olson, L. P., Luo, J., Almarsson, Ö. & Bruice, T. C. Mechanism of aldehyde oxidation catalyzed by horse liver alcohol dehydrogenase. *Biochemistry* **35**, 9782–9791 (1996).
67. Könst, P. et al. Enantioselective oxidation of aldehydes catalyzed by alcohol dehydrogenase. *Angew. Chem. Int. Ed.* **51**, 9914–9917 (2012).
68. Rupp, M. & Görisch, H. Purification, crystallisation and characterization of quinoprotein ethanol dehydrogenase from *Pseudomonas aeruginosa*. *Biol. Chem. Hoppe. Seyler* **369**, 431–440 (1988).
69. Wehrmann, M. & Klebensberger, J. Engineering thermal stability and solvent tolerance of the soluble quinoprotein PedE from *Pseudomonas putida* KT2440 with a heterologous whole-cell screening approach. *Microb. Biotechnol.* **11**, 399–408 (2018).
70. Schmidt, S., Christen, P., Kiefer, P. & Vorholt, J. A. Functional investigation of methanol dehydrogenase-like protein XoxF in *Methylobacterium extorquens* AM1. *Microbiology* **156**, 2575–2586 (2010).
71. Good, N. M., Moore, R. S., Suriano, C. J. & Martinez-Gomez, N. C. Contrasting in vitro and in vivo methanol oxidation activities of lanthanide-dependent alcohol dehydrogenases XoxF1 and ExaF from *Methylobacterium extorquens* AM1. *Sci. Rep.* **9**, 4248 (2019).

72. Hying, Z. T., Rushmer, A. M., Loh, C. Y., Bruger, E. L. & Bazurto, J. V. *Methylobacterium extorquens* PA1 utilizes multiple strategies to maintain formaldehyde homeostasis during methylotrophic growth. *PLOS Genet.* **21**, e1011736 (2025).
73. Catalano, A. et al. Aldehydes: what we should know about them. *Organics* **5**, 395–428 (2024).
74. Friedrich, H. B. The oxidation of alcohols to aldehydes or ketones. *Platin. Met. Rev.* **43**, 94–102 (1999).
75. Enache, D. I., Knight, D. W. & Hutchings, G. J. Solvent-free oxidation of primary alcohols to aldehydes using supported gold catalysts. *Catal. Lett.* **103**, 43–52 (2005).
76. Besson, M. & Gallezot, P. Selective oxidation of alcohols and aldehydes on metal catalysts. *Catal. Today* **57**, 127–141 (2000).
77. Najafishirtari, S. et al. A perspective on heterogeneous catalysts for the selective oxidation of alcohols. *Chem. – Eur. J.* **27**, 16809–16833 (2021).
78. Jiang, Y. et al. Multigene editing in the *Escherichia coli* genome via the CRISPR-Cas9 system. *Appl. Environ. Microbiol.* **81**, 2506–2514 (2015).
79. Datta, S., Costantino, N. & Court, D. L. A set of recombineering plasmids for gram-negative bacteria. *Gene* **379**, 109–115 (2006).
80. Baba, T. et al. Construction of *Escherichia coli* K-12 in-frame, single-gene knockout mutants: the Keio collection. *Mol. Syst. Biol.* **2**, 2006.0008 (2006).
81. Han, J., Lin, K., Sequeira, C. & Borchers, C. H. An isotope-labeled chemical derivatization method for the quantitation of short-chain fatty acids in human feces by liquid chromatography–tandem mass spectrometry. *Anal. Chim. Acta* **854**, 86–94 (2015).
82. Kiefer, P., Schmitt, U. & Vorholt, J. A. eMZed: an open source framework in Python for rapid and interactive development of LC/MS data analysis workflows. *Bioinformatics* **29**, 963–964 (2013).
83. Zhou, Z. et al. A new decoupling method for accurate quantification of polyethylene copolymer composition and triad sequence distribution with 13C NMR. *J. Magn. Reson.* **187**, 225–233 (2007).
84. Shaka, A. J., Keeler, J. & Freeman, R. Evaluation of a new broadband decoupling sequence: WALTZ-16. *J. Magn. Reson. 1969* **53**, 313–340 (1983).
85. Nash, T. The colorimetric estimation of formaldehyde by means of the Hantzsch reaction. *Biochem. J.* **55**, 416–421 (1953).
86. Madeira, F. et al. The EMBL-EBI Job Dispatcher sequence analysis tools framework in 2024. *Nucleic Acids Res.* **52**, W521–W525 (2024).
87. Huerta-Cepas, J., Serra, F. & Bork, P. ETE 3: reconstruction, analysis, and visualization of phylogenomic data. *Mol. Biol. Evol.* **33**, 1635–1638 (2016).
88. Rozewicki, J., Li, S., Amada, K. M., Standley, D. M. & Katoh, K. MAFFT-DASH: integrated protein sequence and structural alignment. *Nucleic Acids Res.* **47**, W5–W10 (2019).
89. Waterhouse, A. M., Procter, J. B., Martin, D. M. A., Clamp, M. & Barton, G. J. Jalview Version 2—a multiple sequence alignment editor and analysis workbench. *Bioinformatics* **25**, 1189–1191 (2009).
90. Minh, B. Q. et al. IQ-TREE 2: new models and efficient methods for phylogenetic inference in the genomic era. *Mol. Biol. Evol.* **37**, 1530–1534 (2020).
91. Bianchini, G. & Sánchez-Baracaldo, P. TreeViewer: flexible, modular software to visualise and manipulate phylogenetic trees. *Ecol. Evol.* **14**, e10873 (2024).
92. Goujon, M. et al. A new bioinformatics analysis tools framework at EMBL-EBI. *Nucleic Acids Res.* **38**, W695–W699 (2010).
93. Sievers, F. et al. Fast, scalable generation of high-quality protein multiple sequence alignments using clustal omega. *Mol. Syst. Biol.* **7**, 539 (2011).
94. Robert, X. & Gouet, P. Deciphering key features in protein structures with the new endscript server. *Nucleic Acids Res.* **42**, W320–W324 (2014).
95. Abramson, J. et al. Accurate structure prediction of biomolecular interactions with AlphaFold 3. *Nature* **630**, 493–500 (2024).
96. Flamholz, A., Noor, E., Bar-Even, A. & Milo, R. eQuilibrator-the biochemical thermodynamics calculator. *Nucleic Acids Res.* **40**, D770–D775 (2012).
97. Noor, E., Haraldsdóttir, H. S., Milo, R. & Fleming, R. M. T. Consistent estimation of Gibbs energy using component contributions. *PLOS Comput. Biol.* **9**, e1003098 (2013).
98. Noor, E. et al. Pathway thermodynamics highlights kinetic obstacles in central metabolism. *PLoS Comput. Biol.* **10**, e1003483 (2014).
99. Noor, E. et al. An integrated open framework for thermodynamics of reactions that combines accuracy and coverage. *Bioinformatics* **28**, 2037–2044 (2012).
100. Beber, M. E. et al. eQuilibrator 3.0: a database solution for thermodynamic constant estimation. *Nucleic Acids Res.* **50**, D603–D609 (2022).
101. Noor, E., Flamholz, A., Liebermeister, W., Bar-Even, A. & Milo, R. A note on the kinetics of enzyme action: a decomposition that highlights thermodynamic effects. *FEBS Lett.* **587**, 2772–2777 (2013).
102. Hektor, H. J., Kloosterman, H. & Dijkhuizen, L. Identification of a magnesium-dependent NAD(P)(H)-binding domain in the nicotinoprotein methanol dehydrogenase from *Bacillus methanolicus*. *J. Biol. Chem.* **277**, 46966–46973 (2002).

Acknowledgements

We would like to express our gratitude to Miriam Bortfeld-Miller, Philipp Christen and Patrick Kiefer for technical support. This work was supported by ETH Zurich and the Swiss National Science Foundation (310030B-201265 and 10.002.015) (to J.A.V.).

Author contributions

P.K., E.H., M.A.R., D.H., and J.A.V. conceived the study. P.K., L.A.B., A.M.O., and T.B. assessed the formate production of fully methylotrophic and methanol-dependent strains. E.H. and H.S. purified proteins and performed the in vitro experiments. B.J. performed the Mdh screen. E.H., H.S., B.J., and L.A.B. performed adaptation experiments. P.K., B.J., and L.A.B. performed LC-MS analysis. B.J. performed HPLC analysis. S.H.R. performed NMR analysis. P.K., E.H., and J.A.V. wrote the manuscript, with contributions from all authors.

Competing interests

The authors P.K., B.J., and J.A.V. filed a patent based on overoxidizing and non-overoxidizing methanol dehydrogenases (application no. EP25176751.3). Other authors do not claim competing interests.

Additional information

Supplementary information The online version contains supplementary material available at https://doi.org/10.1038/s41467-025-65949-9.

Correspondence and requests for materials should be addressed to Philipp Keller or Julia A. Vorholt.

Peer review information *Nature Communications* thanks Yongjin Zhou and the other, anonymous, reviewer(s) for their contribution to the peer review of this work. A peer review file is available.